Chemical and temporal manipulation of early steps in protein assembly tune the structure and intermolecular interactions of protein-based materials

Valeria Italia[1*], Amanda Jons[2,3*], Bhavika Kaparthi[2], Britt Faulk[4,5], Marco Maccarini[6], Paolo Bertoncello[7], Ken Meissner[1], Don Martin[6], and Sarah E. Bondos[2,3,4]

[1]Department of Physics, Swansea University, Swansea, Wales.
[2]Department of Cell Biology and Genetics, Texas A&M Health Science Center, Texas A&M University, Bryan, TX 77807, USA.
[3]Interdisciplinary Graduate Program in Genetics, Texas A&M University, College Station, TX 77843, USA.
[4]Department of Medical Physiology, School of Medicine, Texas A&M University, Bryan, TX 77807, USA
[5]Department of Biochemistry and Biophysics, Texas A&M University, College Station, TX 77843, USA
[6]University Grenoble Alpes, SyNaBi, TIMC-IMAG/CNRS/INSERM, UMR 5525, Grenoble, F-38000, France.
[7]Department of Chemical Engineering, Swansea University, Swansea, Wales.

***Valeria Italia and Amanda Jons have contributed equally and are joint first authors.**

Correspondence
Ken Meissner (current address)
Department of Metallurgical, Materials, and Biomedical Engineering
University of Texas at El Paso
El Paso, Texas, USA.
Email: kemeissner@utep.edu

Don Martin
University Grenoble Alpes
SyNaBi, TIMC-IMAG/CNRS/INSERM, UMR 5525
Grenoble, F-38000, France
Email: don.martin@univ-grenoble-alpes.fr

Sarah Bondos
Department of Medical Physiology
School of Medicine
8447 Riverside Pkwy, 1359 TAMU
Texas A&M University
Bryan, TX 77807
bondos@tamu.edu

Running Title: Tuning the structure of protein-based materials

Page Counts:
Total Manuscript: 26 Pages
Supplementary Material: 6 Pages

Tables: 1 Page
Figures: 5 Pages

Abstract

The *Drosophila* intrinsically disordered protein Ultrabithorax (Ubx) undergoes a series of phase transitions, beginning with noncovalent interactions between apparently randomly organized monomers, and evolving over time to form increasingly ordered coacervates. This assembly process ends when specific dityrosine covalent bonds lock the monomers in place, forming macroscale materials. Inspired by this hierarchical, multi-step assembly process, we analyzed the impact of protein concentration, assembly time, and subphase composition on the early, noncovalent stages of Ubx assembly, which are extremely sensitive to their environment. We discovered that in low salt buffers, we can generate a new type of Ubx material from early coacervates using 5-fold less protein, and 100-fold less assembly time. Comparison of the new materials with standard Ubx fibers also revealed differences in the extent of wrinkling on the fiber surface. A new image analysis technique based on autocorrelation of Scanning Electron Microscopy (SEM) images was developed to quantify these structural differences. These differences extend to the molecular level: new materials form more dityrosine covalent cross-links per monomer, but without requiring the specific tyrosine residues necessary for crosslinking previously established materials. We conclude that varying the assembly conditions represents a facile and inexpensive process for creating new materials. Most new biopolymers are created by changing the composition of the monomers or the method used to drive assembly. In contrast, in this study we used the same monomers and assembly approach, but altered the assembly time and chemical environment to create a new material with unique properties.

Keywords: protein-based materials, biomaterials, coacervation, aggregation, self-healing, phase separation, intrinsically disordered proteins

Summary:

The Ultrabithorax (Ubx) protein undergoes a series of phase transitions, progressing from monomers, to random aggregates, to increasingly ordered coacervates which crosslink to form materials. By altering the assembly time and chemical environment, we have stabilized early stages of assembly to generate a new material requiring 5-fold less protein and 100-fold less assembly time and have 3-fold more cross-links per monomer. These materials differ in monomer packing and surface morphology.

1. Introduction

Many intrinsically disordered proteins undergo phase transitions to form assemblies that provide the structural support, create mechanical tension, adhere to surfaces, create strong composite materials, and/or provide the biomechanical cues that direct cell behavior (Boskey & Villareal-Ramirez, 2016; Has et al., 2022; Sun & Kekenes-Huskey, 2023; Shamilov et al., 2021). Inspiration from this biology has stimulated the development of methods to create synthetic protein-based materials for many applications, including drug delivery, tissue engineering, biosensors, cell culture studies and biomedical devices (Lee et al., 2001; Ayoub et al., 2007; Teulé et al., 2009). Each application requires the materials to have the appropriate topology, mechanical properties, and/or porosity for timely chemical/ligand diffusion (Ayoub et al., 2007; Teulé et al., 2009; Wen et al., 2010; Champion et al., 2022; Nilebäck et al., 2018; Bowen et al., 2018; Majithia et al., 2011; Patterson et al., 2015). These properties are determined by the structure of the material. In turn, the structure of the material is determined by the mechanism through which the protein monomers self-assemble.

Several intrinsically disordered proteins, including Collagen, various silks, Mussel Adhesive Protein, and Ultrabithorax (Ubx), have the ability to self-assemble at the air-water interface, forming a film that can be re-arranged into other shapes (Nilebäck et al., 2018; Bowen et al., 2018; Majithia et al., 2011; Patterson et al., 2015; Åstrand et al., 2015; Zhang et al., 2022; Zhang et al., 2017). The formation of the film is the rate-limiting step that establishes many of the intermolecular interactions, and thus the properties, of the final material (Zhang et al., 2022; Zhang et al., 2017). The initial steps of film formation rely on interactions between monomers, and between monomers and aggregates. These interactions are non-covalent and hence very sensitive to the environment (Zhang et al., 2017; Li et al., 2023). Consequently, the chemical and physical conditions present during these early steps has the potential to impact the assembly kinetics, monomer interactions and packing, and ultimately the structure, behavior, and yield of the final macroscale materials.

Here we report such environmental influences on film and material formation utilizing the *Drosophila melanogaster* Hox transcription factor Ultrabithorax (Ubx). Ubx self-assembles in a series of defined steps, and early steps do not involve intermolecular covalent bonds (Majithia et al., 2011; Patterson et al., 2015; Greer et al., 2009; Huang et al., 2010; Huang et al., 2011; Howell et al., 2015). Therefore, these steps have the potential to be influenced by their environment. We also used monomers composed of Ubx that were genetically fused to Enhanced Green Fluorescent Protein (EGFP) (Huang et al., 2011). The resulting fusion protein is termed EGFP-Ubx. In the EGFP-Ubx amino acid sequence, the last amino acid of EGFP and the first amino acid of Ubx are both covalently bound to a short amino acid linker via peptide bonds. Ubx and EGFP-Ubx monomers spontaneously self-assemble *ex vivo* at an air-water interface to form biopolymeric materials (Figure 1) (Greer et al., 2009). During this hierarchical, multistep process, Ubx monomers first form nanoscopic aggregates, which then reorganize to create lines of protein monomers, termed protofibrils (Majithia et al., 2011). Lateral association of protofibrils generates fibrils with a diameter similar to amyloid fibrils, although not amyloid in structure (Greer et al., 2009). Fibrils associate laterally to form a macroscale thin film, which can either be used as is or drawn into biocompatible fibers (Patterson et al., 2015). The properties of the film determine the properties of the resulting fibers: fiber diameter, which ranges from 2 – 400 μm, depends on the thickness of the film, whereas the surface area of the film determines fiber length, which can reach several meters (Huang et al., 2010; Patterson et al., 2014; Patterson et al., 2015).

We used the Langmuir-Blodgett approach to quantify the environmental influences on the early stages of Ubx assembly (Crawford et al., 2014). By varying protein concentration, subphase properties and

assembly times, we discovered a protocol to prolong the lifetime of films composed of randomly packed Ubx, which is an obligatory early intermediate in the Ubx assembly process (Figure 1A). By stabilizing this state, we could draw these early films into fibers, in which dityrosine covalent cross-links locked the protein monomers into a randomly packed configuration. These differences in monomer arrangement ultimately affected the surface structure of the resulting fibers, which we quantified by developing a novel image analysis technique based on autocorrelation of Scanning Electron Microscopy (SEM) images. Compared to existing procedures to prepare fibers from Ubx monomers, these new fiber materials exhibit more than 3-fold more crosslinks per monomer, require 5-fold-less protein, and 100-fold less assembly time to form.

2. Results

2.1 Fiber Structure

Ubx undergoes multiple phase transitions at the air-water interface. First, monomers coalesce into apparently randomly packed, two-dimensional aggregates within minutes. These aggregates reshape into lines of monomers, which interact laterally to form fibrils, and then films. How different are the early randomly arranged films from the later, linearly ordered films? One way to compare the structure of these different phases is to draw them both into fibers, and compare the structure of the fibers. The ordered films can be drawn into fibers with diameters ranging from 2 to 200 μm (Greer et al., 2009). For all experiments on fibers, we used Ubx genetically fused to Enhanced Green Fluorescent Protein (EGFP-Ubx) so that later we can monitor protein density using green fluorescence (Supplemental Material Figure S1). This protein fusion does not impact the Ubx assembly (Tsai et al., 2015). Surprisingly, after a brief 10-minute incubation, the films composed of randomly packed EGFP-Ubx protein aggregates can also be drawn into fibers (Figure 1). Because the films were small and thin compared to films formed later during assembly, the fibers were also thinner and more difficult to lift from the film surface. Using 2 nmol plain Ubx protein over buffer G0, we compared fibers generated after 10, 60, or 120 minutes assembly time. These parameters coincide with the different stages of assembly in our prior electron microscopy experiments (Figure 1).

The surfaces of the resulting fibers are clearly different (Figure 2). As films are drawn into fibers, folds in the film create wrinkles visible on the fiber surface. Films exhibiting irregular edges have difficulty merging into a single, gap-free structure as the surface is compressed. Such films produce fibers with visible discontinuities, appearing as pits or unaligned wrinkles on the surface. While fibers created after a 10-minute incubation present some pits and knobs, the visible wrinkles are mostly aligned. Fibers obtained after waiting 60 minutes, during which the film reorganizes, display a non-continuous and winding pattern of wrinkles. We suspect that the lack of long-range order in the fibers reflects the lack of long range order and the small, discontinuous shape of the films. Finally, fibers obtained after an ordered, linear film has formed at 120 minutes incubation have deep, aligned wrinkles. Deeper wrinkles and larger folds are consistently created from films that are thicker and/or more highly crosslinked. Thus, there is a clear correlation between the properties of the surface film and the nature of the fibers drawn from that film.

To quantify these observations, we used both autocorrelation and wavelet analysis. Autocorrelation analysis evaluates the extent of overlap as one image is moved vertically across another. An example of a perfectly autocorrelated sample is a series of parallel straight lines (Figure 3A). Imagine placing two copies of this image, one above the other, and then sliding the top image down across the other image. Before the images overlap, aspects of the image (white vs. black) do not overlap, and the y-axis value is 0. When the parallel lines in the image first begin to overlap, signal is generated when any black pixels overlap other

black pixels, or white overlaps white. The more the images overlap, the larger percentage of each line is in registration and the higher the value of the y-axis in the autocorrelation graph. When the image and its copy are perfectly aligned, then all points on one image correlate with its copy on the other image and the y-axis value is 1. As the images then begin to move apart the auto-correlation decreases, which is a reverse of the prior process. If a random image is subjected to this same analysis, then the only correlation observed as the images begin to overlap would occur by random chance as light or dark pixels happen to overlap. This random level of correlation would occur less frequently, but would increase as the images overlap to a greater extent, because there are more opportunities for two overlaid pixels to have the same coloration. Thus, on the autocorrelation graph, the lines to either side of X = 0 have a steeper slope. When the two random images overlay perfectly (Vertical Translation Position is 0), suddenly all points are correlated, yielding a spike of height 1. Thus, the autocorrelation graph of a well-correlated image will appear like a cone and have a large width at half the maximum height (red line in Figure 3B), whereas a poorly correlated image will appear as a spike embedded in a short cone, and thus have a very small width at half height. Because the lines depicted in panel A are oriented in the same direction as the movement of the image, all of the lines (or, in our analysis, wrinkles) do not need to be the same width to be well correlated. The top and bottom of a consistently wide wrinkle will still correlate, as will the top and bottom of a thin wrinkle.

Autocorrelation graphs for Ubx fibers formed from films incubated for 10, 60, or 120 minutes are shown in Figure 3D-F, respectively. Fibers drawn after allowing film to form for 10 minutes yielded an autocorrelation graph in which the full width at half maximum height (FWHM) was 4.34 µm. As expected, autocorrelation analysis of the 60-minute fibers yields a smaller FWHM of 2.48 µm, indicating a more disorganized surface. This disorganization of the fiber surface originates from the 60-minute films, indicating that these films were not as well-packed compared to the films present at 10 minutes. This poor packing is consistent with disassembly of the initial randomly organized film (Figure 1B), which has not yet reorganized. Finally, fibers generated from film incubated for 120 minutes, which has had the opportunity to re-organize into laterally interacting linear aggregates, exhibited the most organization, with a significant increase in the structural linearity and continuity (FWHM = 8.72 µm).

The autocorrelation data determines the extent to which large features (here, wrinkles) persist over long distances (10s of µm) in the fibers. In other words, is a wrinkle that is wide the top of the microscopy image still wide at the bottom of that same image? To identify repetitive features that persist over smaller distances, a wavelet analysis was performed across a 0.1 µm horizontal slice across each fiber. The advantage of the wavelet analysis is that the analysis can identify changes in spatially repeating structures across the fiber. In other words, is a wide wrinkle likely to be adjacent to other wide wrinkles, creating a repeating pattern? If so, in what region of the fiber is this pattern observed?

Similar to a Fourier analysis, a wavelet analysis looks for spatial frequencies, in cycles per distance, within the fiber. A range of frequencies (vertical axis) are tested to determine how well they match the image, and where within the image/slice the match occurs. This method creates a spectrogram in which the vertical axis is the spatial frequency of the structure. The horizontal axis is the distance across the fiber and the color identifies the magnitude of the spatial frequency at each point on the fiber where the analysis is run. The resulting “U-shaped” data starts at the spatial frequency matching the entire width of the fiber (the bottom of the y-axis) and, therefore, only produces one data point positioned at the center of the fiber. As the spatial frequency increases (moving up the vertical axis), the frequency repeats more times across the sample and the number of data points corresponding to that frequency increases.

In the fiber formed after a 10-minute waiting period (Figure 3G), structure (generally wrinkles) with spatial frequencies around a few cycles/μm are identified, as shown by the yellow/green areas on the spectrogram. While some wrinkles are observed across most of the width of the fiber, these structural features are less regular (only green intensity) and only persists for 0.25 – 0.5 μm across the fiber. In the fiber formed after a 60-minute waiting time (Figure 3H), a much smaller fraction of the fiber has surface features and the signal from these features is not as strong. Thus, any wrinkles present lose any semblance of a consistent size or periodicity. In contrast, for the fiber formed after a 120-minute waiting time (Figure 3I), the wrinkles persist across the width of the fiber (green signal). Around 10 μm this signal strengthens (yellow), reflecting well-repeating structures. The repeating structures persist for ~5 μm across the fiber, a long distance relative to the size of Ubx monomer (~5 nm). The analysis clearly shows that the 120-minute fiber displays the most regular structural features, followed by the 10-minute fiber. The 60-minute fiber has a very irregular surface.

These SEM images and analysis by autocorrelation and wavelet experiments demonstrate that the films produced after different incubation times produce fibers with different surface characteristics. It follows that the films that produced these fibers also have different structures. In particular, after 120 minutes of incubation, organized linear arrays of Ubx have formed and had enough time to interact with each other, rotate to minimize gaps, and create larger, more robust films that produce fibers with pronounced, regular wrinkles on the surface. Importantly, wrinkling impacts the ability of cells to attach and migrate on a surface (Dimmock et al., 2020; He & Jiang, 2017). Therefore, techniques that alter the presence, depth, and consistency of wrinkles on the surface of materials may alter cell: material interactions as well.

2.2 Langmuir film formation

We hypothesized that differences observed in the surface of the fibers are caused by changes in the packing of monomers at the film stage. Indeed, prior microscopy experiments suggested that Ubx self-assembles into a random film, then disassembles that structure and reassembles into a new film composed of linear arrays of Ubx (Figure 1). However, these samples had to be manipulated to move them from the surface of a liquid to a form compatible with electron microscopy. To ensure that these differences in monomer packing within films was not an artifact of sample preparation, we observed film formation using the Langmuir technique, which is the premier approach to measure assembly in two dimensions at the air-water interface. In a Langmuir trough, a protein is added to the surface of a subphase liquid, and then the protein is allowed to interact with itself and the air/water interface for a set period of time. Following this incubation, the surface area is reduced by contraction of two movable barriers. As protein aggregates come into contact, phase transitions in the Langmuir film are produced (Li et al., 2019). At the start of the procedure (the lower right side of the pressure-area graphs in Figure 4), the available area per molecule is large, and so the proteins do not interact with each other. This portion of the experiment is termed the “gas phase”. Compressing the monolayer forces the proteins to become more closely packed and commence interactions with each other, creating the “liquid phase”. For Ubx, which forms small films – like islands – of aggregates, the liquid phase begins when small, isolated films are forced into proximity. When the proteins are close to their maximum packing, they have reached the “solid phase”, and any further compression would cause the film to wrinkle or fold over itself (Aveyard et al., 2000a; Aveyard et al., 2000b). Since we are interested in studying the early phases of Ubx assembly, the transition from the gas phase to the liquid phase is of primary interest.

To observe such early phases of assembly, the Langmuir technique generally requires pure water or low salt concentrations in the subphase. The high surface tension of water helps to reduce the interparticle

distance between large molecules or colloids deposited on the surface, thus promoting assembly (Yeon et al., 2008). The addition of salts and sugars to the subphase can further increase the surface tension, potentially driving the system into the liquid or solid phase before compression begins, which would prevent observation of these transitions (Pegram & Record, 2007; Docoslis et al., 2000).

Previously established conditions were optimized to drive Ubx self-assembly. Typically, 15 nmol of Ubx was spread across a 338 cm^2 surface in which the subphase is a high salt buffer (0.5 M NaCl, 0.05 M NaH_2PO_4, 5% w/v D-Glucose pH=8.0) (Mendes et al., 2018). To slow Ubx association and allow us to measure discrete early stages of assembly, we reduced both the amount of protein utilized and the concentration of salts and glucose in the buffer.

These experiments used a fusion protein in which Enhanced Green Fluorescent Protein is covalently attached, via a peptide bond, to a short linker peptide which, in turn, is fused via another peptide bond to the N-terminus of Ubx, creating EGFP-Ubx (Huang et al., 2010) (Supplemental Figure 1). Ubx and EGFP-Ubx self-assemble into materials equally well (Huang et al., 2010; Tsai et al., 2015).

To characterize EGFP-Ubx monomer oligomerization and biopolymeric film formation obtained under different conditions, we used a Langmuir trough to obtain surface pressure–area (π-A) isotherms (Langmuir, 1917; Langmuir & Schaefer, 1938; Blodgett, 1935). The shape of the isotherm depends on the shape and area occupied by the aggregates, which, in turn, depends on nature of the amphiphile (herein, EGFP-Ubx), the compression speed, the spreading conditions, the temperature, and the time allowed for protein assembly prior to barrier compression. To identify appropriate parameters for these experiments, the first tests varied the amount of EGFP-Ubx monomers added to identify conditions under which we can best observe the gas phase to liquid phase transition (Figure 4A) (Crawford & Leblanc, 2014). These experiments used 0.1 M NaCl solution in the subphase and 10-minute assembly time prior to compression. This assembly time was selected to catch the earliest stage of Ubx assembly, based on our electron microscopy data (Figure 1). We tested adding 1, 2, or 4 nmol of EGFP-Ubx to the trough. As expected, when larger amounts of protein are added to the surface, a larger fraction of the surface is covered, yielding higher π-A values and shifting the curve to the right.

We compared the shape of the curves to determine the optimal amount of protein to use in further experiments. In the 4 nmol sample, the curve began rising almost immediately (reading right to left). Therefore, there was too much protein to observe the complete gas to liquid transition, even with the barriers fully open. In contrast, the data from 1 nmol of EGFP-Ubx revealed a large (flat) gas phase and the gas-liquid transition, but only a small portion of the curve represented the liquid phase, hampering data analysis. Furthermore, film was not visible by eye, and fibers could not be reliably drawn from the compressed surface. The curve representing 2 nmol of EGFP-Ubx revealed a complete gas-liquid phase transition and a useful amount of data was present in both the liquid and gas phases of the curve. Thus, all further Langmuir experiments (Figure 2B-D) used 2 nmol protein.

Data were analyzed by calculating the limiting area (LA) from LB curves as the x-axis intercept of the liquid phase portion of the curve (Hann & Kathirgamanathan, 1990; Wu et al., 2020; Watanabe et al., 1988). The higher the number, the larger the area occupied by the film, and the greater the yield of materials. Importantly, the LA is linearly dependent on the amount of protein added (Figure 4A, inset). This relationship demonstrates that the data are reproducible, and that there are no concentration-dependent processes (e.g. adhesion to the trough) that could confound interpretation of the results.

By using the Langmuir technique to assess early stages of assembly, we are restricted to a subphase with a low saline content. However, altering the salinity has the potential to impact the behavior and stability of proteins, especially proteins such as Ubx with a high density of charged residues. The amino

acid sequence of Ubx includes a 60-amino acid homeodomain (Supplemental Figure 1), which has a predicted net charge of +11. This portion of the protein requires counterions to prevent charge repulsion from disrupting the protein's structure, leading to aggregation. Prior studies demonstrate that Ubx solubility is indeed sensitive to salt concentration: While Ubx is soluble in in a low salt buffer like 20 mM Tris, 100 mM KCl, halving or removing the KCl from this buffer causes some Ubx aggregation (Bondos & Bicknell, 2003). However, in prior aggregation studies, Ubx was mixed into these low salt buffers, instead of being dissolved in a high salt buffer and then applied to the surface of a low salt buffer, as in a Langmuir trough. To examine the effects of the salinity of the subphase, we compared the assembly of 2 nmol of EGFP-Ubx following a 10-minute incubation on the surface of (i) water, (ii) 100 mM NaCl (low saline), or (iii) 100 mM NaCl and 50 mM NaH_2PO_4, pH = 8.0 (buffered low saline) (Figure 1B). As for other proteins (Mendes et al., 2024; Booth et al., 2024), fusion to EGFP improves Ubx solubility (Tsai et al., 2015). However, white precipitate was still observed when using water as the subphase. The loss of a portion of the Ubx molecules to aggregation partially accounts for the small amount of film formed when water was used as a subphase (Figure 4B). Although a visible precipitate did not form when 100 mM NaCl was used as the subphase, less film was formed in saline-only solution than when phosphate buffer was added to the sample. This reduced ability to assemble could be due to loss of protein to micro-aggregation, or to EGFP-Ubx monomers adopting a conformation that was less able to self-assemble.

A critical question is whether Langmuir experiments, using a low salt subphase, can reproduce the same or similar stages of assembly that were observed by SEM (Figure 1) (Majithia et al., 2011). If the ability of Ubx to assemble, disassemble, and reassemble films is independent or not strongly dependent on salt concentration, then we should be able to reproduce these assembly steps, first observed by electron microscopy, in our Langmuir experiments. If Ubx still undergoes a disassembly step during film formation, we would observe a reduction in the surface area covered by the film - the LA - during the disassembly stage. To search for a disassembly step during film formation on low-salt subphases, we compared the behavior of EGFP-Ubx films as a function of assembly time. The range of selected assembly times spanned those previously established for assembly of Ubx films and fibers (Figure 1) (Greer et al., 2009).

Our initial experiments used the low saline subphase (0.1M NaCl) (Figure 4C, Table 1). Relative to the 10 minute experiment, the 60 minute surface pressure–area (π-A) isotherm exhibited a large leftward shift, corresponding to a large reduction in film size as measured by LA (at 60 minutes, LA = 209 ± 3 versus 271 ± 2 cm^2 at 10 minutes). This reduction is consistent with the de-polymerization of the randomly organized Ubx film observed by EM (Figure 1), and the irregular surface features of fibers formed by 60 minute films (Figure 2). After a 120 minute incubation, the film has re-grown and exceeds the size of the 10 minute film (LA = 417 ± 4 cm^2). The depolymerization/repolymerization is easily visible on a graph of LA vs polymerization time (Figure 4C inset, Table 1).

If depolymerization is a necessary step in Ubx assembly, then we should also observe a leftward shift of the pressure-area isoform at shorter incubation times in the buffered saline solution. To test this hypothesis, 2 nmol of EGFP-Ubx was added to a buffered subphase (50 mM NaH_2PO_4, 100 mM NaCl pH=8.0) and allowed to incubate for 10, 30, 60, or 120 minutes (Figure 4C, Table 1). Relative to the 10 min isotherm, the 30 minute isotherm also shifted to the left, consistent with the disassembly of random aggregates previously observed by electron microscopy[8]. Likewise, the LA was also reduced from 416 ± 7 cm^2 to 296 ± 5 cm^2. By 60 min incubation the film had regrown to match its initial (10 min) size, with an LA = 433 ± 5 cm^2. The film continued to expand, though at a reduced rate, at longer incubation times, again mimicking observations in high salt conditions. After 120 min incubation, the LA reached 489 ± 3 cm^2. Thus, this assembly behavior is non-monotonic with time.

Importantly, the low salt subphase seems to not only permit formation (and subsequent disassembly) of the random aggregates, but also extends the lifetime of these aggregates. After 60 min incubation, the aggregates formed on 0.1 M NaCl are still disassembling (Figure 4D), but have already re-assembled when phosphate buffer is included in the solution (Figure 4C) and in buffers with higher salt concentrations (Figure 1). Given that Ubx first forms random aggregates during self-assembly in both high salt conditions (Figure 1) and low salt conditions (Figure 4), we conclude that the random aggregates are an obligatory step in Ubx assembly.

An unusual feature appeared inconsistently in the surface pressure-area isotherms in several of these experiments. Large bumps were sometimes observed on the right side of the isotherm, before reaching the gas/liquid transition. Examples include the 60 and 120 minute isotherms in Figure 4C and the 10 minute isotherm in Figure 4D. We attribute these bumps to re-orientation of films during compression. As the random aggregates disassemble and re-form using linear protein aggregates, the films become very long and thin. Under surface compression, surface pressure forces the films to rotate such that their narrow axis is parallel to the direction of compression, thus relieving some of the pressure.

2.3 Monomer density and extent of crosslinking

We were surprised that fibers were able to be drawn from films incubated for short periods of time (e.g., 10 min when using a weak saline subphase, Figure 2). The data thus far suggest that these films are composed of random aggregates of Ubx rather than the organized lines of Ubx monomers that form with longer incubation periods. If the organization of Ubx monomers is different in films using low protein concentrations, a 0.1M NaCl subphase, and short times compared to the standard high protein concentration, high salt buffer, and long incubation times (condition abbreviated pbt, Figure 5I), then the internal organization of monomers in the resulting fibers should be different as well. These packing differences are expected to alter the interfaces between Ubx monomers within the films and fibers, which, in turn, will impact how the proteins crosslink to stabilize the solid materials.

We used confocal microscopy to compare the amount of Ubx cross-linking in materials formed using different protocols. During materials assembly, Ubx monomer-monomer interactions are reinforced by the spontaneous formation of dityrosine covalent bonds (Figure 5C,D). These dityrosine bonds fluoresce blue (Figure 5A), and contribute to the mechanical strength of the materials (Howell et al., 2015; Watanabe et al., 1988). Thus, fibers with the brightest blue fluorescence contain more dityrosine bonds, and are stronger. Many materials exhibit direct links between their structure and their mechanical properties (Wegst et al., 2015; Grindy et al., 2015). We quantified blue fluorescence to determine whether similar interactions are formed using the two different methods (Figure 3). Because Ubx films are very thin, it is challenging to reliably quantify fluorescence from dityrosine bonds. Therefore, we created thicker fibers from the Ubx films. Touching a narrow object to the surface of the film causes the film to adhere, lift, and reshape itself into a fiber. To reduce the inner filter effect and allow quantitative measurement of fluorescence on cylindrical fibers, confocal microscopy was used to image a thin slice of intact fibers (Figure 5A).

Because fibers formed using pbt conditions have less long-range order (Figure 5H) and can contain gaps or pits, they may appear less fluorescent because these areas lack protein, instead of due to a difference in the arrangement of proteins. By using EGFP-Ubx fusion monomers (Huang et al., 2011; Tsai et al., 2015) to make the materials, we were able to normalize the intensity of blue fluorescence for the amount of green fluorescence provided by EGFP, and thus the amount of protein being imaged. This approach also

normalizes the data for differences in fiber size and any expansion or contraction of the fibers caused by the different salt concentrations.

When fibers are drawn using films assembled using high salt and protein concentrations for longer time periods (PBT conditions, Figure 5), only six of the sixteen tyrosines are able to form dityrosine bonds (Watanabe et al., 1988). This is because the portions of the surface of a Ubx monomer that interface with other monomers are restricted by the ordered arrangement of Ubx monomers into lines during film assembly.

We compared the dityrosine bond content (blue fluorescence / green fluorescence) for fibers made using the conditions identified in this work (designated pbt in Figure 5H) versus previously established conditions (PBT). The blue fluorescence, and therefore the content of dityrosine bonds, was much higher for the pbt fibers than the PBT fibers (Figure 5F). To determine whether incubation time, or protein concentration and subphase composition had the largest impact on dityrosine bond formation, we also made PBt fibers (high amount of EGFP-Ubx used, high salt buffer, short incubation time), and pbT fibers (low EGFP-Ubx used, low salt subphase, long incubation time). While all parameters affected the dityrosine bond content, the protein concentration and subphase composition clearly had the largest effect.

The increased fluorescence of pbt fibers compared to PBT fibers could be due to (i) an increased fraction of Ubx monomers forming the previously discovered dityrosine bonds in the materials, or (ii) the formation of additional, currently unidentified, dityrosine bonds (Patterson et al., 2014). To distinguish these possibilities, we compared dityrosine bond formation in fibers formed by a Ubx tyrosine mutant. In PBT conditions, only 6 of the 16 tyrosines in the Ubx sequence are capable of forming dityrosine bonds (Howell et al., 2015). In the mutant Y4S/Y12S, the tyrosines (abbreviated Y) at amino acid positions 4 and 12 are mutated to serine (S) (Figure 5E), preventing these positions from forming dityrosine bonds with their obligatory partner amino acids, Y296 and Y293, respectively. If the increased fluorescence of fibers generated using pbt conditions is due to an increased fraction of monomers forming already identified dityrosine bonds, then the Y4S/Y12S Ubx should reduce the fluorescence of materials generated using pbt conditions. However, if this increased fluorescence is due to other bonds forming, these mutations will have little effect on the overall fluorescence.

Based on our Langmuir data (Figure 2), we had hypothesized that under pbT conditions, Ubx was forming films composed of linear arrays of protein, just as it does when assembled using PBT conditions (Figure 1). Indeed, the Y4S/Y12S mutation reduces the fluorescence of fibers formed under pbT conditions, verifying that the films/fibers observed after long periods of time in Figure 2 rely on the same dityrosine bonds as Ubx materials formed under standard, high salt conditions (Trillo et al., 1972). However, fibers formed using Y4A/Y12S Ubx assembled for short times (pbt conditions) remained as fluorescent as the pbt fibers composed of wild-type Ubx, indicating that the tyrosines at position 4 and 12 are not needed for dityrosine bond formation under these conditions. Therefore, pbt conditions promote the formation of a different set of dityrosine bonds, and organization of monomers in these materials is fundamentally different than in Ubx materials formed under previously established (PBT) conditions.

4. Discussion

By changing the environmental conditions during the formation of Ubx materials, we have stabilized a different phase of Ubx assembly, ultimately creating different materials using the same monomers and the same technique. Although many proteins, including Ubx, are capable of forming covalent crosslinks, the initial interactions that drive assembly are non-covalent. Thus, these interactions are also extremely sensitive to the environment. The early stages of Ubx assembly into a material involves initially the

formation of randomly organized aggregates prior to disassembly of that film and repacking Ubx into linear arrays (Figure 1). We discovered that these aggregates are an obligatory intermediate, and that controlling assembly time and buffer composition stabilizes different types of Ubx film. These experiments verified that the aggregates observed using electron microscopy were not an artefact of sample preparation, and verified that the random Ubx aggregates, once formed, must undergo a disassembly process to create linear protein arrays. Thus, the random aggregates can also be viewed as a kinetic trap on the high-salt assembly pathway. The Langmuir experiments also identified conditions that prolong the longevity of the randomly packed aggregates, allowing them to form films which could be drawn into fibers. These differences in monomer organization cause fibers created from these films to also exhibit different surface structures, wrinkling to different extents. Wrinkles can guide cell topology and cell-materials interactions, and are thus anticipated to be useful for applications such as regenerative medicine, drug delivery, and antimicrobial surfaces (Izawa et al., 2018; Nguyen et al., 2020; Dimmock et al., 2020).

If the organization of monomers is different in these two types of films, we reasoned that their ability to form covalent crosslinks to stabilize and strengthen the resulting materials may also be different. In the linearly organized films formed in high salt, only 6 of the 16 tyrosines in the Ubx amino acid sequence are positioned to form dityrosine covalent bonds. We quantified the extent to which both fibers generated from low-salt or high-salt films were able to fluoresce blue, a hallmark of dityrosine bonds. These experiments demonstrated that the less organized film/fibers actually form more dityrosine bonds. An increase in the number of dityrosine bonds could be due to a greater percentage of Ubx monomers forming the 6 known bonds, or to the alternative packing of Ubx monomers allowing a greater variety of bonds to form. Point mutations removing specific tyrosines (Y4 and Y12) that participate in the formation of known dityrosine bonds dramatically reduced the amount of blue fluorescence in high salt fibers, as expected. However, these mutations had little impact on the fluorescence of materials produced in low salt. Therefore, materials formed using pbt conditions are able to create dityrosine bonds that are inaccessible when assembling in PBT conditions.

Other groups have reported manipulating protein assembly by altering the physicochemical conditions. The environment can shift either monomer conformation or the preferred monomer-monomer interfaces for assembly, thus driving the formation of different materials using the same monomers. For example, altering the assembly time, temperature or UV-light exposure of supramolecular polymers creates particles of different sizes and topologies (Yagai et al., 2019). For a recombinant spider silk protein, changing the buffer used for assembly alters tyrosine rigidity and generates fibers with improved mechanical properties (Stengel et al., 2023). Many smart materials are designed to depolymerize in response to changes in environmental conditions such as pH, temperature, redox status, light, etc. (Li et al., 2023). These changes in morphology potentiate the controlled delivery of drugs by triggering loading (materials assembly) and unloading (materials disassembly) conditions. This idea has been extended to transition materials between different, but still assembled, morphologies. For instance, using materials composed of a PDMS/silk bilayer can reversibly switch between a smooth and a wrinkled surface using light, temperature and mechanical stretching as stimuli (Wang et al., 2019).

With growing advancements in medicine, the need for sophisticated, functionally complex biomaterials has been increasing (Huebsch & Mooney, 2009). Distinct tasks require materials with specific morphologies, mechanical properties, and biological functions. Therefore, generating, varying, and controlling these traits is critical to meeting this need. The most common approach to altering materials is to change the chemical composition of the monomers from which they are formed (e.g., Hedhammar et al., 2010; Howell et al., 2015; Roberts et al, 2020). For instance, varying the number and density of

elastin motifs in elastin-like peptides allows the creation of microparticles with different complex geometries, such as core-shell, hollow shell, and porous particles (Roberts et al., 2020).

5. Conclusion

We have demonstrated that protein assembly conditions can be altered to manipulate monomer-monomer interactions and the organization of monomers within a material, resulting in materials with significantly different properties. Materials formed in low salt conditions exhibit more dityrosine covalent cross-links. Since the mechanical strength of these fibers is generated from dityrosine bonds (Huang et al., 2010), we would also expect these fibers to be stronger. Furthermore, increased cross-linking is expected to decrease pore size and impact the diffusion of ligands through these materials. Importantly, the activity of a protein (EGFP) genetically fused to Ubx is also preserved during assembly in these low salt conditions. Therefore, this new method does not impede functionalization of these materials via gene fusion. Importantly, the activity of the added protein is preserved and even stabilized in protein materials (Howell et al., 2016; Tsai et al., 2015; Huang et al., 2011; Mendes et al, 2024; Booth et al., 2024). Numerous fusion proteins have been created which incorporate different types of protein activities (e.g. cell binding peptides, cytokines, enzymes and ligand binding proteins) (Huang et al., 2011; Howell et al., 2016). These bioactive materials have the potential to impact in numerous biomedical fields including use in wound healing, drug delivery, tissue engineering, and sensing (Rosenbloom et al., 1993; Wagenseil & Mecham 2009).

To fully leverage materials composed of these fusion proteins, the properties of the materials, such as strength and ligand diffusion rate, must match the needs of the intended application. Such properties are most frequently adjusted by either changing the composition of the monomer or by selecting a different method to promote assembly. Importantly, the different materials analyzed herein were generated using the same monomers and the same overall assembly technique. We were able to create a variety of materials by altering the chemical environment because Ubx undergoes hierarchical, multi-scale self-assembly in which non-covalent bonds dictate the initial monomer-monomer interactions. This approach to creating new materials does not require new monomers to be designed, and manufactured, nor does it need new equipment or additional experts. Because Ubx shares these traits with many other materials-forming proteins (Revell et la., 2021; Jehele et al., 2018), we anticipate that altering the assembly conditions could change the structure of many other protein-based materials.

2. Materials and Methods

2.1 EGFP-Ubx protein Expression and Purification

Following previously described techniques, the EGFP-Ubx fusion protein was cloned into the pET19b vector (Novagen) and transformed into Rosetta(DE3)pLysS *E. coli* cells (Novagen) (Majithia et al., 2011; Patterson et al., 2014; Howell et al., 2015). Cells were cultured overnight in Luria Broth (LB) containing 50 µg/mL ampicillin and 30 µg/mL chloramphenicol, at 37°C. *E. coli* cell culture (8 mL) was used to inoculate 1 L of LB media, which was fermented until reaching an optical density at 600 nm between 0.6 and 0.8. EGFP-Ubx protein expression was then induced with 1 mM isopropyl b-D-1-thiogalactopyranoside (IPTG) at 26°C prior to another overnight fermentation. Cells were harvested using 30 minutes of centrifugation at 4°C. The collected pellet was stored at -20°C.

Each pellet was lysed in 40 mL of lysis buffer (50 mM sodium phosphate buffer, pH 8.0, 5% glucose w/v, 500 mM NaCl, 1 Roche Complete Mini Protease Inhibitor Cocktail tablet, 0.8 mg/L DNase I) for 20 minutes and centrifuged at 4°C for 30 minutes. The supernatant was loaded in a 10 mL nickel−nitrilotriacetic acid

(Ni-NTA) agarose resin column (Fisher), which was previously equilibrated with 50 mL of G0 buffer (50 mM sodium phosphate buffer, pH 8.0, 5% glucose w/v, 500 mM NaCl). The column was iteratively washed with 10 column volumes of G0 buffer containing 0, 20, 40 and 80 mM imidazole. The purified proteins were eluted with 25 mL of G0 buffer containing 300 mM Imidazole and stored at -20°C.

The concentration of EGFP-Ubx proteins was calculated from the absorbance of EGFP using the Lambert-Beer law using an extinction coefficient of 56 $(mM\ cm)^{-1}$ at 488 nm (Tsien, 1998).

2.2 Generation of EGFP-Ubx Fibers

Fibers were collected from the Langmuir tray or the "buffer reservoir" tray using a 10 µL sterile plastic inoculation loop with the handle cut away as previously described (Patterson et al., 2014). The loop was touched gently on the surface of the buffer and moved away to pull the fiber from the EGFP-Ubx surface film. Since the film is composed of nanoscale fibrils, withdrawing the plastic loop slowly allows a microscale fiber to be drawn from the surface film and wrapped around the loop which acts as a support. The resulting fiber-wrapped loop was immobilized in a sterile plastic petri dish to slowly dehydrate the fibers, and stored at room temperature until use.

The diameter and length of pulled fibers can be varied by adjusting protein concentration and assembly time, an approach that enables the production of materials with different properties. Fibers narrower than 10 µm extend elastically, with breaking strength and Young's modulus decreasing with increasing diameter. For fibers with diameters greater than 15 µm, in contrast, an increase in diameter is followed by a proportional increase in breaking strain, typical plastic deformation behavior (Huang et al., 2010).

2.3 Scanning Electron Microscopy (SEM)

SEM images were recorded with a Hitachi S4800 FE-SEM operating at V = 1 kV and I = 5 µA. The samples were fixed to a specimen holder (SEMClip, 32 x 10mm, M4 cylinder mount, 2 clips from Agar Scientific). To obtain a uniform image without noise, we also used double-sided carbon tape to further stabilize the sample. No coating was needed for the fibers since Ubx-based materials are weakly conductive.

2.4 Image analysis

The alignment and uniformity of the wrinkle components were analyzed with an in-house developed MATLAB code. A description of the code and the code itself is included in Supplemental Information. An axial autocorrelation was employed to identify large scale continuity in structural features (*i.e.* wrinkles on the surface of the fibers). The full width at half of the maximum height (FWHM) of the resulting graph was used to quantify the long-range alignment. The FWHM is correlated with long-range order. If the wrinkles are well ordered, they stay aligned during the axial autocorrelation, creating a wide FWHM. If the wrinkles are randomly distributed, the alignment deteriorates quickly during the axial autocorrelation and results in a narrow FWHM. Therefore, the FWHM of the autocorrelation trace is a measure of the fiber structure with a larger FWHM indicating long-range ordered structure to the fiber.

A continuous wavelet transform using a standard Morse basis wavelet was used to visualize the spatial periodicity across the wrinkles. This analysis can detect local repeated patterns that may not extend through the length of the fiber. To increase the signal to noise ratio, the pixel intensities were averaged over a 0.1 µm longitudinal section of the fiber. The results are displayed in a color-coded scalogram where a higher magnitude (more yellow) indicates a strong relation of that frequency around that area of the fiber. In addition, by looking at which frequencies are present in the signal, the approximate size of the wrinkles can be determined by taking the inverse of the frequency (Supplemental Figure 1).

2.5 Langmuir Technique and Limiting Area Analysis

Our protocols were based on previous studies using Bovine Serum Albumin (BSA) (Crawford & Leblanc 2014), which has a molecular weight similar to that of EGFP-Ubx. The measurements of π-A isotherms were carried out on a KSV NIMA Langmuir Large KN2003 (PTFE; total area 841 cm^2) equipped with a dipping well and a dipping mechanism. All solutions and buffers were prepared using deionized water purified using a Milli-Q (18 mΩ.cm) purification system. The Langmuir trough was cleaned prior to use with warm water and acetone to remove any trace contaminants. The trough was filled with water or saline solution as indicated. With the barriers fully open, specified amounts of stock spreading solution (purified EGFP-Ubx protein diluted to 10 mM in purified water) was added to the subphase surface using the microspreading technique (Terauchi et al., 2020; Hussain et al., 2018), in which small drops of protein were added directly and symmetrically across the surface of the trough. Proteins were allowed to equilibrate for varying times, as indicated, before beginning barrier compression at a rate of 25 cm^2/min and at room temperature. The π-A isotherms of Ubx proteins were measured to investigate the effects of three critical parameters: concentration of EGFP-Ubx, buffer in which EGFP-Ubx is dissolved, and assembly time after protein introduction. A minimum of 3 replicates were completed for each condition. In each panel, data were collected with the same protein preparation and on the same day to avoid the influence of weather on laboratory environmental conditions and, hence, materials assembly. Unlike water insoluble molecules like lipids, proteins such as Ubx are partially soluble in water. Thus, some fraction of the protein added to the surface will dissolve in the subphase. Consequently, the x-axis of the pressure-area isotherms is reported as cm^2 instead of nm^2/molecule, a standard practice for experiments involving soluble proteins (Pal et al., 2011). The limiting area was calculated by extrapolating the linear part of the curve to the x-axis (Hann & Kathirgamanathan, 1990; Wu et al., 2020; Watanabe et al., 1988).

2.6 Confocal Microscopy

Confocal microscopy was used to compare the density of blue-fluorescent dityrosine bonds in Ubx materials formed under different conditions. In EGFP-Ubx fibers, the green fluorescence provided by the EGFP component correlated with the density of protein within the materials and was used to normalize the dityrosine data. Since fibers have different sizes, the fluorescence intensity was also normalized to fiber diameter. In this way we compared measurements derived from different samples (Howell et al., 2016; Crawford & Leblanc 2014).

Fiber samples were collected for confocal microscopy analysis from different trays in which the buffer, protein concentration, and incubation time were varied. As indicated, some fibers were assembled using a low protein concentration in a 100 mM NaCl buffer (a condition termed “PB” herein) while other fibers were assembled using a high protein concentration in Buffer G0 (PB condition). Buffer G0 contains 5% glucose w/v, 500 mM NaCl, 50 mM sodium phosphate buffer, pH 8.0. Fibers were collected after either a 10-minute incubation time or an overnight incubation for each condition. Fibers were air-dried overnight before being imaged with a Nikon Eclipse Ti A1R inverted confocal microscope equipped with NIS Elements AR 4.10.01 software to analyze fluorescent intensity of both the DAPI (488 nm) and FITC (405 nm) channels. All data were averaged from at least 3 separate fibers, and each fiber was measured 3 independent times. Thus, each LA value reflects a minimum of 9 measurements. Microscope settings were constant, and all images were taken with a 20x objective using the FITC channel at a gain of 52 and DAPI channel at a gain of 120.

Supplementary Material Description. Supplementary Material contains a schematic of the EGFP-Ubx protein fusion used in this study (Supplmental Figure 1), and a detailed description of the SEM linearity analysis, including the code.

Acknowledgements. The authors gratefully acknowledge members of the Meissner, Martin, and Bondos laboratories for helpful discussions, and Andrew Fisher for assistance with developing the MatLab Code for image analysis. VI was funded by a Cotutelle Fellowship from the ubBIO project, funded by the IDEX Strategic Alliance between University Grenoble Alpes (France) and Swansea University (UK).

References

Åstrand C, Chotteau V, Falk A, Hedhammar M. Assembly of FN-silk with laminin-521 to integrate hPSCs into a three-dimensional culture for neural differentiation. Biomater Sci. 2020;8:2514-2525.

Aveyard R, Clint JH, Nees D, Paunov VN. Compression and structure of monolayer of charged latex particles at air/water and octane/water interfaces. Langmuir. 2000a;16:1969-1979.

Aveyard R, Clint JH, Nees D, Quirke N. Strcture and collapse of particle monolayers under lateral pressure at the octane/aqueous surfactant solution interface. Langmuir. 2000b;16:8820-8828.

Ayoub NA, Garb JE, Tinghitella RM, Collin MA, Hayashi CY. Blueprint for a high-performance biomaterial: full-length spider draglline silk genes. PLoS One. 2007;2:e514.

Blodgett KB. Films built by depositing successive monomolecular layerws on a solid surface. J Am Chem Soc. 1935;57:1007-1022.

Booth RM, Jons A, Gong X, Banerjee S, Faulk B, Rye H, Bystroff C, Bondos SE. Immonbilization and enhancement of a heterodimeric fluorescence biosensor in fibrous protein biomaterials. Prot Sci. 2024, in press.

Bondos SE, Bicknell A. Detection and prevention of protein aggregation before, during, and after purification. Anal Biochem. 2003;16:223-231.

Boskey AL, Villareal-Ramirez E. Intrinsically disordered proteins and biomineralization. Matrix Biol. 2016;52-54:43-49.

Bowen CH, Dai B, Sargent CJ, Bai W, Ladiwala P, Feng H, Huang W, Kaplan DL, Galazka JM, Zhang F. Recombinant spidroins fully replicate primary mechanical properties of natural spider silk. Biomacromolecules. 2018;19:3853-3860.

Champion JA, Pho T. Surface engineering of protein nanoparticles modulates transport, adsorption, and uptake in mucus. ACS Appl Mater Interfaces. 2022;14:51697-51710.

Crawford NF, Leblanc RM. Serum albumin in 2D: a Langmuir monolayer approach. Adv. Colloid Interface Sci. 2014;207:131-138.

Dimmock RL, Wang X, Fu Y, El Haj AJ, Yang Y. Biomedical applications of wrinkling polymers. Recent Prog Mater. 2020;2:1-31.

Docoslis A, Giese RF, van Oss CJ. Influence of the water-air interface on the apparent surface tension of aqueous solutions of hydrophilic solutes. Colloids and Surfaces B: Biointerfaces. 2000;19:147-162.

Hann RA, Kathirgamanathan P. Molecules for Langmuir-Blodgett film formation [and discussion]. Philos Trans R Soc London Ser A, Math Phys Sci. 1990;330:141.

Fan L, Li J-L, Cai Z, Wang X. Bioactive hierarchical silk fibers created by bioinspired self-assembly. Nat Commun. 2021;12:2375.

Greer AM, Huang Z, Oriakhi A, Lu Y, Lou J, Matthews KS, Bondos SE. The Drosophila transcription factor

Ultrabithorax self-assembles into protein-based biomaterials with multiple morphologies. Biomacromolecules. 2009;10:829-837.

Grindy SC, Learsch R, Mozhdeli D, Cheng J, Barrett DG, Guan Z, Messersmith PB, Holten-Andersen N. Control of hierarchical polymer mechanics with bioinspired metal-coordination dynamics. Nat Mater. 2015;14:1210-1216.

Has C, Sivadas P, Das SL. Insights into membrane curvature sensing and membrane remodeling by intrinsically disordered proteins and protein regions. J Membr Biol. 2022;255:237-259.

He X, Jiang Y. Substrate curvature regulates cell migration. Phys Biol. 2017;14:035006.

Hedhammar M, Bramfeldt H, Baris T, Widhe M, Askarieh G, Nordling K, von Aulock S, Johansson J. Sterilized recombinant spider silk fibers of low pyrogenicity. Biomacromolecules. 2010;11:953-959.

Hessinger C, Technau GM, Rogulja-Ortmann A. The Drosophila Hox gene Ultrabithorax acts in both muscles and mononeurons to orchestrate formation of specific neuromuscular connections. Development. 2017;144:139-150.

Howell DW, Duran CL, Tsai SP, Bondos SE, Bayless KJ. Functionalization of Ultratbithorax materials with vascular endothelial growth factor enhances angiogenic activity. Biomacromolecules. 2016;17:3558-3559.

Howell DW, Tsai SP, Churion K, Patterson J, Abbey C, Atkinson JT, Porterpan D, You YH, Meissner KE, Bayless KJ, Bondos SE. Identification of multiple dityrosine bonds in materials composed of the Drosophila protein Ultrabithorax. Adv Funct Mater. 2015;25:5988-5998.

Howell D, Tsai SP, Churion K, Patterson J, Bayless K, Bondos SE. Mechanically-tunable, protein-based matreials can be functionalized with other proteins and with DNA. Biophys J. 2016;110:338a.

Huang Z, Salim T, Brawley A, Patterson J, Matthews KS, Bondos SE. Functionalization and patterning of protein-based materials using active Ultrabithorax chimeras. Adv Funct Mater. 2011;21:2633-2640.

Huang Z, Lu Y, Majithia R, Shah J, Meissner K and Matthews KS, Bondos SE, Lou J. Size dictates mechanical properties for protein fibes self-assembled by the Drosophila Hox transcription factor Ultrabithorax. Biomacromolecules. 2010;11:3644-3651.

Huebsch N, Mooney DJ. Inspiration and application in the evolution of biomaterials. Nature. 2009;462:426-432.

Hussain SA, Dey B, Bhattacharjee D, Mehta N. Unique supramolecular assembly through Langmuir-Blodgett (LB) technique. Heliyon. 2018;4:e01038.

Izawa H, Okuda N, Yonemura T, Kuroda K, Ochi K, Ifuku S, Morimoto M, Saimoto H, Noda M, Azuma K, Okamoto Y, Ito N. Application of bio-based wrinkled surfaces as cell culture scaffolds. Colloids Interfaces. 2018;2:15.

Jehele F, Fratzi P, Harrington MJ. Metal-tunable self-assembly of hierarchical structure in mussel-inspired peptide films. ACS Nano. 2018;12:2160-2168.

Langmuir I. The constitution and fundamental properties of solids and liquids. II. Liquids. J Am Chem

Soc. 1917;39:1848-1906.

Langmuir I, Schaefer VJ. Activities of urease and pepsin monolayers. J Am Chem Soc. 1938;60:1351-1360.

Lee CH, Singla A, Lee Y. Biomedical applications of collagen. Int J Pharm. 2001;221:1-22.

Li T, Lilja K, Morris RJ, Brandani GB. Langmuir-Blodgett technique for anisotropic colloids: Young investigator perspective. J Colloid Interface Sci. 2019;540;420-438.

Li Y, Yang G, Gerstweiler L, Than SH, Zhao C-X. Design of stimuli-responsive peptides and proteins. Adv Funct Mater. 2023;33:2210387

Majithia R, Patterson J, Bondos SE, Meissner KE. On the design of composite protein-quantum dot biomaterials via self-assembly. Biomacromolecules. 2011;12:3629-3637.

Mendes GG, Booth RM, Pattison DL, Alvarez AJ, Bondos SE. Generating novel materials using the intrinscially disordered protein Ubx. Methods Enzymol. 2018;611:583-605.

Mendes GG, Faulk B, Kaparthi B, Irion AR, Look Fong B, Bayless K, Bondos, SE. Genetic functionalization of protein-based biomaterials via protein fusions. Biomacromolecules. 2024, in press.

Nguyen DHK, Bazaka O, Bazaka K, Crawford RJ, Ivanova EP. Three-dimensional hierarchical wrinkles on polymer films: from chaotic to ordered antimicrobial topographies. Trends Biotechnol. 2020;38:558-571.

Nielsen SB, Lapierre A, Anderson JU, Pedersen UV, Tomita S, Andersen LH. Absorption spectrum of the green fluorescent protein chromophore anion in vacuo. Phys Rev Lett. 2001;87:228102.

Nilebäck L, Arola S, Kvivk M, Paananen A, Linder MB, Hedhammar M. Interfacial behavior of recombinant spider silk protein parts reveals cues on the silk assembly mechanism. Langmuir. 2018;34:11795-11805.

Patterson JL, Abbey CA, Bayless KJ, Bondos SE. Materials composed of the Drosophila melanogaster protein Ultrabithorax are cytocompatible. J Biomed Mater ResA. 2014;102:97-104.

Pal P, Kamilya T, Mahato M, Talapatra GB. Protein monolayer formation at air-electrolyte interaface; A Langmuir-Blodgett study. Surface Rev Lett. 2011;18:267-279.

Patterson JL, Arenas-Gamboa AM, Wang TY Hsiao HC, Howell DW, Pellois JP, Rice-Ficht A, Bondos SE. Materials composed of the Drosophila Hox protein Ultrabithorax are biocompatible and nonimmunogenic. J Biomed Mater Res A. 2015;103:1546-1553.

Pegram LM, Record MT Jr. Hofmeister salt effects on surface tension arise from partitioning of anions and cations between bulk water and the air-water interface. J Phys Chem B. 2007;117;5411-5417.

Revell CK, Jensen OE, Shearer T, Lu Y, Holmes DF, Kadler KE. Collagen fibril assembly: New approaches to unanswered questions. Mater Biol. 2021;12:100079.

Roberts S, Miao V, Costa S, Simon J, Kelly G, Shah T, Zauscher S, Chilkoti A. Complex microparticle architectures from stimuli-responsive intrinsically disordered proteins. Nat Commun. 2020;11:1342.

Rosenbloom J, Abrams WR, Mecham R. Extracellular matrix 4: the elastic fiber. FASEB J. 1993;7:1208-1218.

Shamilov R, Robinson VL, Aneskievich BJ. Seeing keratinocyte proteins through the looking glass of intrinsic disorder. Int J Mol Sci. 2021;22:7912.

Stengel D, Saric M, Johnson HR, Schiller T, Diehl J, Chalek K, Onofrei D, Scheibel T, Holland GP. Tyrosine's unique role in the hierarchical assembly of recombinant spider silk proteins: From spinning dope to fibers. Biomacromolecules. 2023;24:1463-1474.

Sun B & Kekenes-Huskey PM. Myofilament-associated proteins with intrinsic disorder (MAPIDs) and their resolution by computational modeling. Q Rev Biophys. 2023;56:e2.

Terauchi Y, Tanaka T, Mitsuishi M, Yabu H, Yoshimi A, Nantani K, Abe K. Analysis of the self-assembly process of Aspergillus orzyae hydrophobin RolA by Langmuir-Blodgett method. Biosci Biotechnol Biochem. 2020;84:678-685.

Teulé F, Cooper AR, Furin WA, Bittencourt D, Rech EL, Brooks A, Lewis RV. A protocol for the production of recombinant spider silk-like proteins for artificial fiber spinning. Nat Protoc. 2009;4:341-355.

Trillo JM, Jado EI, Fernández SG, Pedrero PS. Monolayers of human serum albumin. Kolloid-Zeitschrift Zeitschrift für Polym. 1972;250:325-329.

Tsai SP, Howell DW, Huang Z, Hsiao HC, Lu Y, Matthews KS, Lou J, Bondos SE. The effect of protein fusions on the production and mechanical properties of protein-based materials. Adv Funct Mater. 2015;25:1442.

Tsien RY. The green fluorescent protein. Annu Rev Biochem. 1998;67:509-544.

Wagenseil JE, Mecham RP. Vascular extracellular matrix and arterial mecchanics. *Physiol Rev*. 2009;**89**:958-989.

Wang Y, Kim BJ, Peng B, Li W, Wang Y, Li M, Omenetto FG. Controlling silk fibroin conformation for dynamic, responsive, multifunctional, micropatterned surfaces. Proc Natl Acad Sci USA. 2019;116:21361-21368.

Watanabe M, Kosaka Y, Oguchi K, Sanui K, Ogata N. Regulation of supermolecular structure of amphiphilic polymers by means of the Langmuir-Blodgett technique. Macromolecules. 1988;21:2997-3003.

Wegst UGK, Bai H, Saiz E, Tomsia A, Ritchie RO. Bioinspired structural materials. Nat Mater. 2015;14:23-36.

Wen H, Lan X, Zhang Y, Zhao T, Wang Y, Kajiura Z, Nakagaki M. Transgenic silkworms (bombyx mori) produce recombinant spider dragline silk in cocoons. Mol Biol Rep. 2010;37:1815-1821.

Wu Y, Fan H, Yang C, Zhang L Pyrene-based amphiphile regulated C_{60} aggregation in monolayers and Langmuir-Blodgett films. Colloids Surfaces A Physicochem Eng Asp. 2020;585:124111

Yagai S, Kitamoto Y, Datta S, Adhikari B. Supramolecular polymers capable of controlling their topology. Acc Chem Res. 2019;52:1325-1335.

Yeon W-C, Kannan B, Wohland T, Ng V. Colloidal crystals from surface-tension-assisted self-assembly: A novel matrix for single-molecule experiments. Langmuir. 2008;24:12142-12149.

Zhang S, Liu Y, Machatschek R, Lendlein A. Ultrathin collagen type I films formed at the air-water interface. MRS Advances. 2022;7:56-62.

Zhang F, Xie G, Pan J. Tunable adsorption and film formation of mussel adhesive protein by potential control. Langmuir. 2017;33: 8749-8756.

Tables

Table 1. Comparison of limiting areas for Ubx films obtained from 2 nmol EGFP-Ubx using a Langmuir apparatus with different incubation times and subphases.

	Water	**0.1 M NaCl**			**0.1 M NaCl + 0.05 M NaH_2PO_4**			
Time (min)	10	10	60	120	10	30	60	120
LA (cm^2)	128 ± 1	271 ± 2	209 ± 3	417 ± 4	416 ± 7	296 ± 5	456 ± 6	503 ± 5

Figure Legends

Figure 1. Hierarchical assembly of Ubx materials. (A) About 15min after dilution into a tray, Ubx begins to form irregular aggregates (red arrow). (B) Within 1h, these aggregates begin to spontaneously reshape into lines of Ubx proteins, termed protofibrils. (C) After 1h, the protofibrils align in parallel and begin to form side-to-side contacts. (D) After 1-2h multiple protofibrils condense to form fibrils about 50 nm in diameter (white arrow). Fibrils also interact laterally to form films which can be lifted from the surface (E). Alternately, films on the air–water interface can be drawn into fibers composed of aligned fibrils (F). (A–C) 100-nm thick carbon films were placed on the surface of the Ubx solution, lifted using TEM grids, stained with 2% w/v phosphotungstic acid and imaged by TEM. (D) A film was transferred to a metal stub, sputter coated in gold, and imaged by scanning electron microscopy. Panels (A)–(C): Adapted with permission from Majithia et al., 2011. Copyright 2011 American Chemical Society. Panel (D): Panel D adapted with permission from Greer et al, 2009. Copyright 2009 American Chemical Society.

Figure 2. Fibers drawn from a Langmuir trough with 2 nmol Ubx in G0 buffer and assembling for (A) 10 minutes, yielding a fiber diameter of 4.5 ± 1.0 μm, (B) 60 minutes to generate a fiber with a diameter of 43 ± 3 μm and (C) 120 minutes (26 μm ± 2 μm diameter fiber) were imaged using a Scanning Electron Microscope with 1 kV voltage. These diameters reflect the area of the film, film thickness, and the density of protein within the film.

Figure 3. Ideal case of perfectly aligned fibers (A) and the corresponding autocorrelation (B) and wavelet analysis (C). Autocorrelation from representative fibers with 10 (D), 60 (E), and 120 (F) minutes of wait time prior to starting the compression of the Langmuir trough. The FWHM is marked by the red line and the value is provided aside the line. Wavelet analysis of the fibers reveals lateral uniformity and wrinkle sizes for assembly times of 10 (G), 60 (H), and 120 minutes (I).

Figure 4. Isothermal compression curves of EGFP-Ubx. (A) 10-minute assembly times, 0.1 M NaCl buffer at different protein concentrations. (B) 10-minute assembly times, 2 nmol protein in different buffers. (C) 2 nmol EGFP-Ubx with different assembly times in 0.1 M NaCl solution. (D) 2 nmol EGFP-Ubx with different assembly times in 0.1 M NaCl+ 0.05 M NaH_2PO_4 pH= 8.0 subphase. Bumps in these curves that occur before (to the right of) the gas-liquid transition have been attributed to rotation of long, thin islands of films, allowing them to pack in parallel as the surface is compressed.

Figure 5. Confocal microscopy of Ubx fibers reveals blue fluorescence of dityrosine bonds (A) and green fluorescence of EGFP (B), in which white scale bars represent 20 μm. Structures of tyrosine (C), dityrosine (D), and serine (E). Normalized fluorescent intensity of EGFP-Ubx fibers for all conditions (F), and for conditions pbt and pbT comparing regular and mutant Ubx fibers. (G) Comparison of the impact of the Y4S/Y12S double mutation on the fluorescence of plain Ubx fibers created from randomly packed films (pbt conditions) and linearly packed films (pbT conditions). (H) Scanning Electron Microscope image of EGFP-Ubx fiber generated in pbt conditions, as defined in (I), a chart listing details of conditions used to create fibers for fluorescence experiments.

Figures

Figure 1

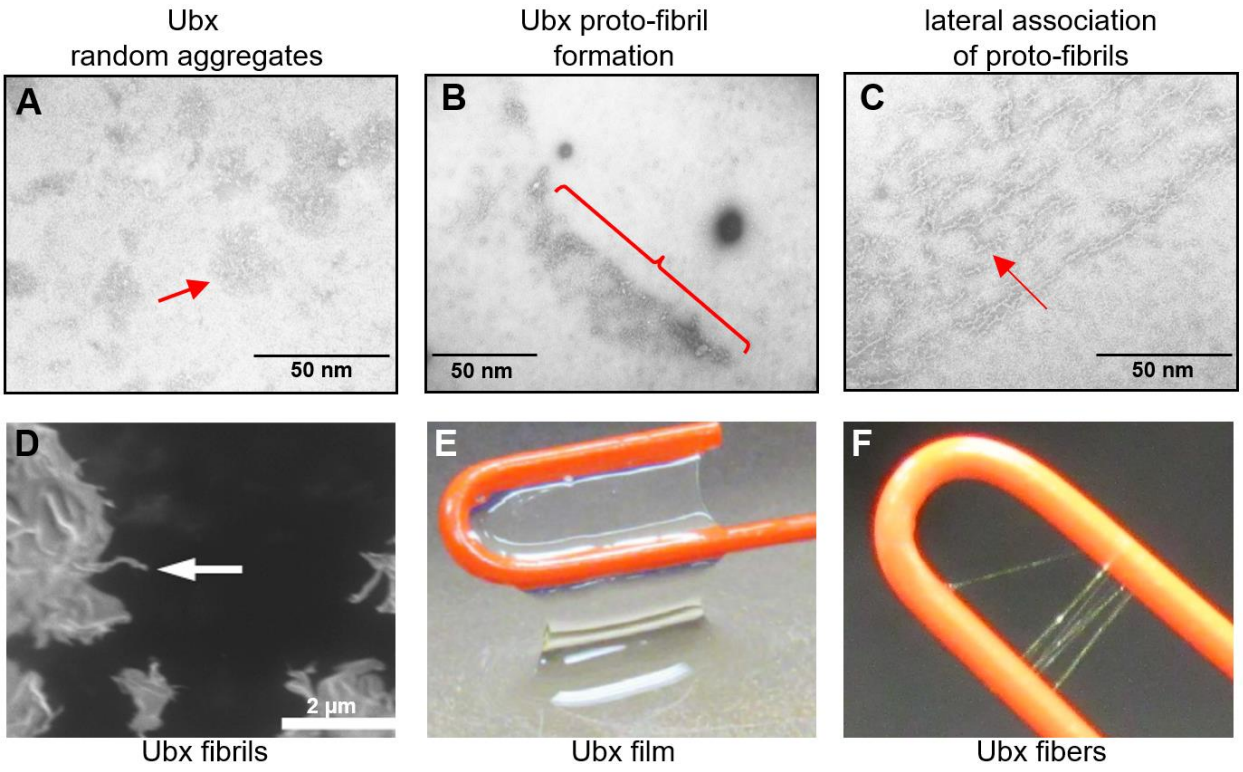

Figure 2

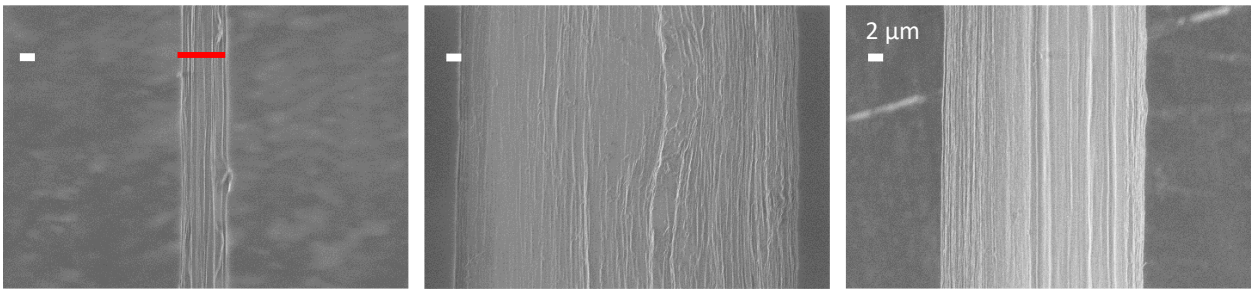

Figure 3

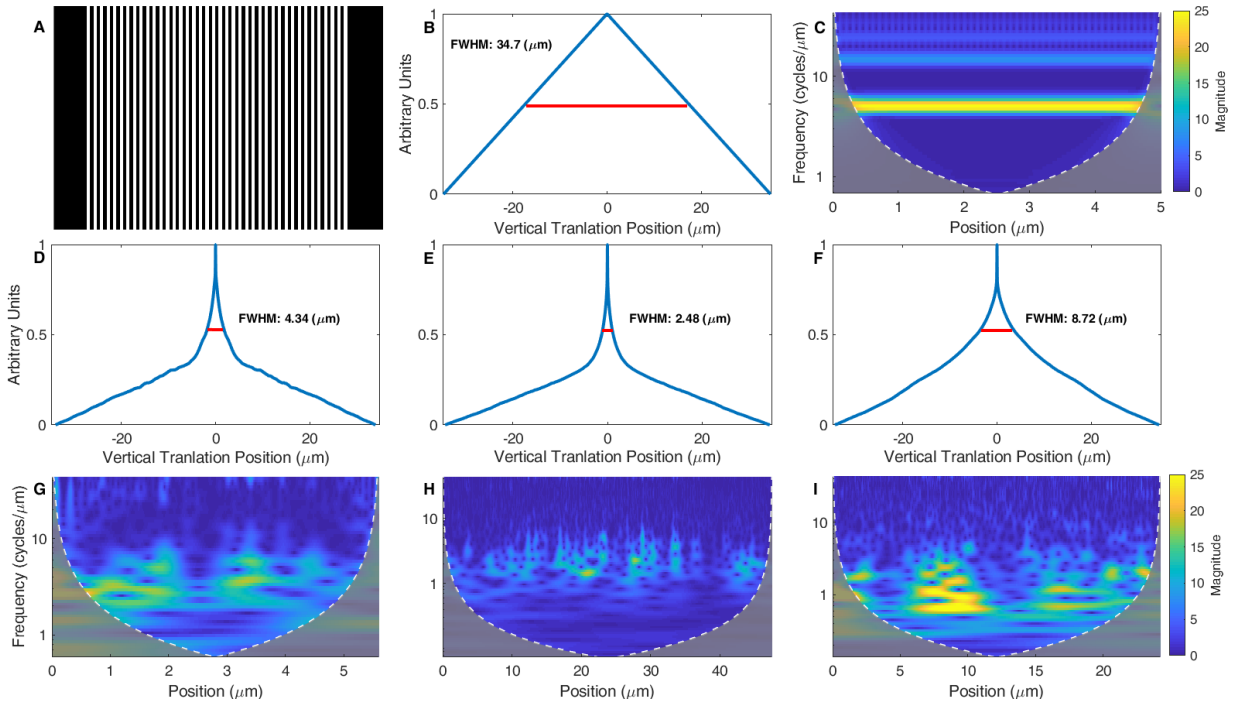
A
B
FWHM: 34.7 (μm)
Arbitrary Units
Vertical Tranlation Position (μm)
C
Frequency (cycles/μm)
Position (μm)
Magnitude
D
FWHM: 4.34 (μm)
Arbitrary Units
Vertical Tranlation Position (μm)
E
FWHM: 2.48 (μm)
Vertical Tranlation Position (μm)
F
FWHM: 8.72 (μm)
Vertical Tranlation Position (μm)
G
Frequency (cycles/μm)
Position (μm)
H
Position (μm)
I
Position (μm)
Magnitude

Figure 4

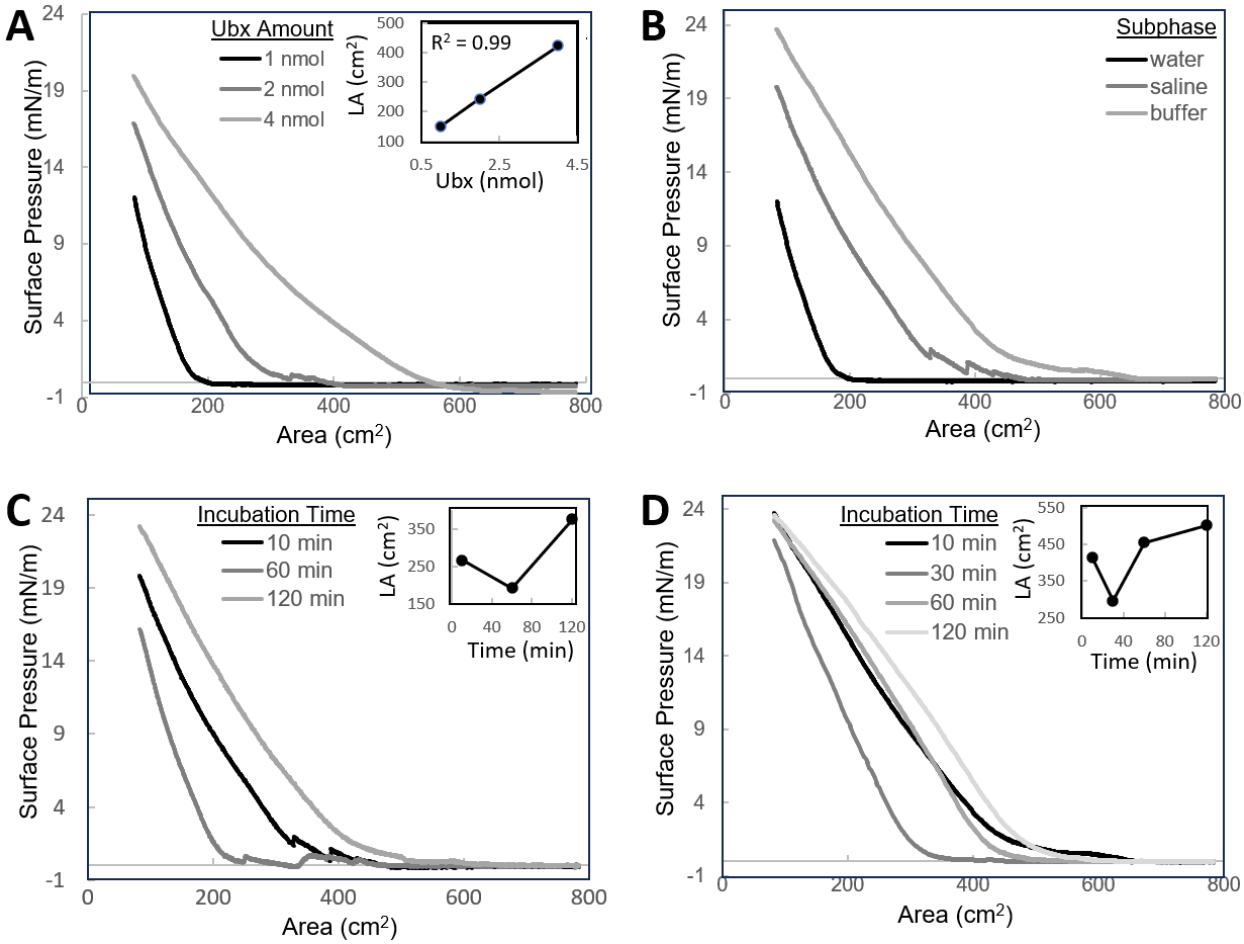
A
Ubx Amount
1 nmol
2 nmol
4 nmol
LA (cm²)
R² = 0.99
Ubx (nmol)
Surface Pressure (mN/m)
Area (cm²)
B
Subphase
water
saline
buffer
C
Incubation Time
10 min
60 min
120 min
Time (min)
D
Incubation Time
10 min
30 min
60 min
120 min
Time (min)

Figure 5

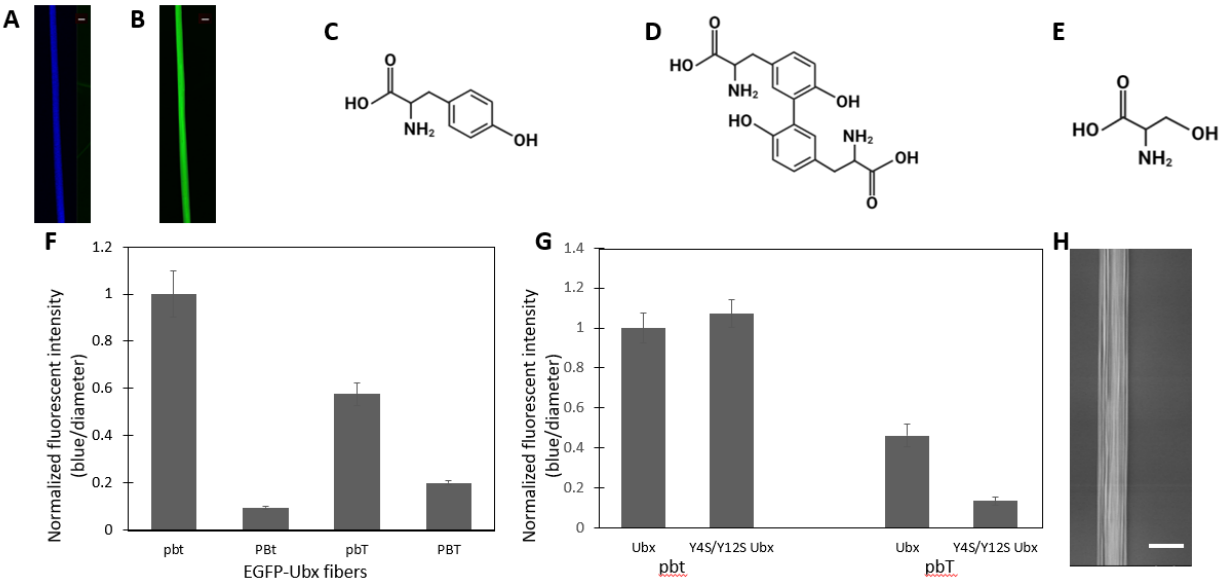

I

Protein	Buffer Used	Time
p: 2 nmol	b: 100 mM NaCl, pH = 7.5	t: 10 minutes
P: 50 nmol	B: 500 mM NaCl + 50 mM NaH_2PO_4 + 5% Glucose, pH = 8	T: overnight